Additive Manufacturing 56 (2022) 102916

Contents lists available at ScienceDirect

Additive Manufacturing

journal homepage: www.elsevier.com/locate/addma

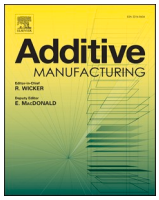

Research paper

A novel approach for powder bed-based additive manufacturing of compositionally graded composites

Zongwen Fu [a,c,*,1], Jihui Ye [a,c,*,1], Martin Franke [b], Carolin Körner [a,b,c]

[a] Friedrich-Alexander University Erlangen-Nürnberg, Joint Institute of Advanced Materials and Processes, Dr.-Mack-Straße 81, Fürth 90762, Germany
[b] Neue Materialien Fürth GmbH, Dr.-Mack-Str. 81, Fürth 90762, Germany
[c] Friedrich-Alexander University Erlangen-Nürnberg, Department of Materials Science, Chair of Materials Science and Technology for Metals, Martensstrasse 5, Erlangen 91058, Germany

ARTICLE INFO

Keywords:
Functionally Graded Materials (FGM)
Electron Beam Powder Bed Fusion (EB-PBF)
Copper tungsten
Particle size distribution
Layer thickness

ABSTRACT

In this feasibility study, a novel selective powder raking approach is used for Electron Beam Powder Bed Fusion (EB-PBF) to produce fully dense and compositionally graded composites. The adaption of the chemical composition along the thickness direction of the printed parts is based on the application of a powder blend composed of powders with different particle sizes combined with varying layer thicknesses during EB-PBF. The microstructure of EB-PBF-processed samples with a composition gradient is investigated. The distribution of different phases in the as-built samples is discussed. Based on the results derived in this work, this approach can be easily extended to other powder bed-based AM technologies as well as to other material systems to produce functionally graded materials.

1. Introduction and conceptualization

Since the proposal of the concept of Additive Manufacturing (AM) at the end of the 20th century, this technology has been attracting increasing attention and research interests for the production of high-performance metallic components [1,2]. Based on the layer-upon-layer build principle, not only the high geometric complexity of produced components but also a sophisticated tailoring of the local material properties (e.g., local chemical composition and microstructure features) can be achieved using AM. So far, using Laser Metal Deposition (LMD), multi-material composites and even Functionally Graded Materials (FGM) with a gradual change in composition along the build direction have been fabricated [3–5]. During LMD, the chemical composition of the layer being printed is easily adjustable via varying the feed rates of different raw materials. Nevertheless, the geometric accuracy and complexity of LMD-processed objects are usually limited.

Compared to LMD, powder bed-based AM approaches, such as Laser Powder Bed Fusion (L-PBF) and Electron Beam Powder Bed Fusion (EB-PBF), allow for the fabrication of high-performance components with excellent printing precision and almost unlimited geometric freedom [6]. Commonly, a pre-alloyed metallic powder with a chemical composition nearly identical to the final printed products is used for EB-PBF and L-PBF to print samples with uniform properties. Recently, in order to tailor the local chemical composition of intermetallic TiAl, resulting in various local microstructural and mechanical properties, different process parameters were used for EB-PBF utilizing a pre-alloyed TiAl powder, which led to selective evaporation of aluminum during EB-PBF under vacuum conditions [7–9]. However, based on this targeted heterogeneous evaporation during EB-PBF, only the local composition fraction of volatile elements (e.g., Al) can vary in a limited range. Currently, in industry and academia, considerable efforts have been made in the field of machine development for EB-PBF as well as L-PBF to fabricate multi-material composites with a large composition gradient and even FGM [10–18].

In 2021, Aerosint, a company located in Belgium, reported successful AM of multi-material components using a selective powder deposition system based on rotating drums for L-PBF taking place in an inert gas atmosphere [10]. The powder particles are held on a patterning drum and selectively deposited at desired locations. As each drum holds and deposits an individual powdered material, several drums can simultaneously be used for L-PBF to build multi-material parts (e.g., Cu-based alloy + stainless steel) [10]. Nevertheless, no reports show whether

* Corresponding authors at: Friedrich-Alexander University Erlangen-Nürnberg, Joint Institute of Advanced Materials and Processes, Dr.-Mack-Straße 81, Fürth 90762, Germany.
E-mail addresses: zongwen.fu@fau.de (Z. Fu), jihui.ye@fau.de (J. Ye).
[1] These authors contributed equally to this work

https://doi.org/10.1016/j.addma.2022.102916
Received 23 February 2022; Received in revised form 13 May 2022; Accepted 21 May 2022
Available online 25 May 2022

this Aerosint drum-based selective powder deposition system can be used for EB-PBF under vacuum conditions.

At the same time, the NTU AM lab (Singapore) and the Fraunhofer Institute IGCV (Augsburg, Germany) developed another interesting powder deposition system: During the L-PBF process in an inert gas atmosphere, the powder hopper that moves above the build platform and delivers powdered feedstock is split into two compartments to create "multiple metal materials" [11,12]. During the powder deposition procedure, for each individual powder, a defined amount of powder particles is actively fed onto the substrate through a roller beneath each compartment. Using this "multi-compartment hopper deposition method", L-PBF of multi-metal parts with a macroscopic lamellar structure (e.g., one layer Cu-based alloy + one layer steel) was successful [11]. Nevertheless, the fabrication of FGM with a gradual change in composition along the build direction could be barely achievable owing to the poor mixing effect during powder deposition.

Lin et al. at the Tsinghua University (Beijing, China) developed a special powder feed system for EB-PBF taking place under vacuum conditions [13,19]. Under the action of gravity and vibration, powders (e.g., TiAl and Ti-6Al-4 V) in two different hoppers are delivered into an interim mixing box and homogenized as well as fed onto the build plate [13]. The amounts of different powders delivered into the interim mixing box can be controlled by defining the vibration amplitude. Simultaneously, the composition of each layer can be precisely manipulated. Based on this powder feed principle, the EB-PBF-built Ti-6Al-4 V / TiAl samples showed a high local microstructural homogeneity and a global compositional gradient in the thickness direction [19]. Nevertheless, one of the main challenges associated with the powder feed approach developed by Lin et al. is the reuse / recycling of the non-melted mixed powder, whose exact chemical composition could hardly be determined [13]. In addition, at the institute ISPMS SB RAS (Tomsk, Russia), Filippov et al. developed a unique material feed system combining wire feed and powder bed [15]. An electron beam was used as a heat source to melt powder or wire, so that the chemical composition of each layer could be different [15].

All those previously mentioned methods developed for L-PBF and EB-PBF to fabricate multi-material components are based on the retrofit of the powder delivery system and associated with substantial costs at the software and hardware level. In this work, FGM with a compositional variation along the thickness direction were built by means of EB-PBF under a high vacuum level using a selective raking approach requiring no additional machine modification. The fundamental mechanism of the raking procedure is illustrated in Fig. 1 **b**. As feedstock, a powder blend containing small particles (blue) and big particles (brown), showing significantly different levels of particle size, is used for EB-PBF. From a theoretical point of view, when setting the layer thickness (gap height between the rake blade and the substrate) larger than the size of blue particles, but smaller than the size of brown particles, only the smaller blue particles will remain after raking (Fig. 1 **b**). From a theoretical point of view, the selective raking method is able to produce different composition ranges. When setting the layer thickness high enough, a mixed composition being in the similarity to the composition of the initial powder blend could be derived. If the two powders have an overlap in the particle size distribution, choosing any layer thickness value that lies in the overlap region could result in a unique composition of the raked powder layer; i.e., if the layer thickness and the particle size distribution of the powder blend were adjusted appropriately, the composition of each layer would be precisely controlled in a targeted manner.

In order to realize and verify this selective powder raking concept, an open-source EB-PBF system (Freemelt ONE, Mölndal, Sweden) that allows users to freely define the scan parameters and to adjust the layer thickness of each layer was applied in this study. The Freemelt ONE device is equipped with a build tank and an additional powder feed tank (Fig. 1 **a**). During the raking procedure, the powder feed tank fully filled with powder particles is mechanically lifted, while the build tank is dropped down by a single layer thickness. Simultaneously, powder particles are raked from the feed tank to the build tank (Fig. 1 **a**). Compared to other gravity-based powder deposition methods, which are widely used for EB-PBF, the powder feed approach used in this study shows a significant advantage, when processing a powder blend composed of powder particles exhibiting different levels of size and specific weight. During the common gravity powder feed procedure, finer and heavier particles in the powder blend tend to sediment. Nevertheless, the possible demixing and sedimentation effects are minimized, when using the Freemelt ONE EB-PBF system equipped with two tanks to process a powder mixture.

As raw materials for EB-PBF, a powder blend composed of large copper particles and smaller tungsten particles was prepared and used in this work as a simple exemplary material system. The copper tungsten system was chosen owing to the big difference in the specific weight of W ($\rho_W \approx 19.25$ g/cm^3 [20]) and Cu ($\rho_{Cu} \approx 8.92$ g/cm^3 [21]). The chemical composition of the Cu-W powder blend can be easily determined employing density measurements (e.g., via helium pycnometry,

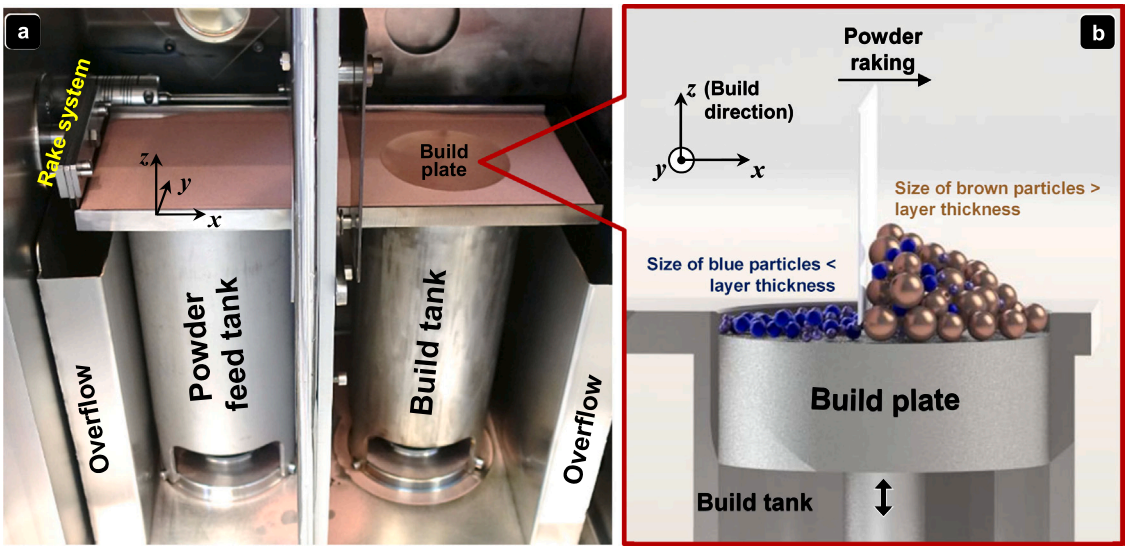

Fig. 1. (a): Build chamber of the Freemelt ONE machine equipped with a rake system and a powder feed tank as well as a build tank, (b):Schematic explanation showing the basic principle of the selective powder raking method.

see Section 2), which is of particular importance to evaluate the homogeneity of the initial powder mixture used for EB-PBF and to recycle the non-molten powder after EB-PBF. In addition, Cu and W are almost not mutually miscible in both solid and liquid states [22]. Therefore, the **in situ** alloying effects and the enthalpy of mixing, which might destabilize the EB-PBF procedure [23,24], are negligible during the printing process. Compared to other conventional Cu-based alloys composed of soluble alloying elements (e.g., Cu-Ni, Cu-Zn etc.) showing good mechanical strength at the expense of electrical conductivity (due to the formation of solid solution), Cu-W could also reach high strength without any compromise in electrical conductivity [25]. Thus, Cu-W composites are currently widely used as contact materials in high voltage interrupters.

This work aims to produce functionally graded Cu-W composite materials via EB-PBF using a Cu-W powder blend composed of elemental Cu and W powders with different levels of particle size and employing the aforementioned selective raking approach. During EB-PBF, the layer thickness was varied. The local microstructure homogeneity and the distribution of different elements of the as-built samples were analyzed and discussed.

2. Material and experimental methods

An inert gas-atomized coarse copper powder (Eckart TLS GmbH, Bitterfeld-Wolfen, Germany) with a spherical particle shape and a finer tungsten powder (Wolfram Bergbau und Hütten AG, St. Martin im Sulmtal, Austria) exhibiting a relative irregular particle morphology were used in this study for EB-PBF. The particle size distribution of the pure copper and the pure tungsten powders was measured by means of **L**aser **D**iffraction **G**ranulometry (**LDG**, Mastersizer 3000, Malvern Panalytical, London, UK). During the particle size measurement, the powder was dispersed in distilled water through stirring. After weighing in a glass bottle and homogenization in a tumbling mixer (Turbulaf ®, Willy A. Bachofen AG, Swiss) without using any grinding media, a powder blend composed of 5 wt % W and 95 wt % Cu (corresponding to 2.4 vol % W and 97.6 vol % Cu) was prepared. To ensure a high homogeneity after tumbling mixing, a small amount of the powder blend was analyzed using a helium pycnometer (pycnomatic ATC EVO, Porotec GmbH, Germany) before EB-PBF. Through helium pycnometry, the true skeletal material density is determined according to the ideal gas law. If the true density of the small amount of the powder blend measured by means of the helium pycnometry significantly differed from the theoretical value, further mixing procedures were performed. In addition, the particle morphology and the flowability of both pure elemental powders as well as the powder blend were investigated utilizing a **S**canning **E**lectron **M**icroscope (SEM, NanoLab 600 DualBeam, FEI - Quanta 450, USA) and a flowability measuring gauge (University Erlangen, Germany), respectively.

EB-PBF was carried out on the Freemelt ONE machine (Fig. 1 **a**) under vacuum conditions ($\sim 10^{-5}$ mbar) without using any additional process gas. After raking the first powder layer onto the preheated start plate composed of pure copper, the surface of the raked powder layer is heated using a defocused electron beam. The temperature of the bottom side of the copper start plate was measured by means of a thermocouple and was displayed as powder bed temperature. During the whole EB-PBF process, this "powder bed temperature" was held at ~400 °C by preheating the freshly raked powder layer. During the selective melting procedure using a focused electron beam with a diameter of ~300 μm, cross-snake hatching with a line offset of 100 μm was applied; the hatching direction was rotated by 90° after each layer; the scan speed and the beam power were set to 809 mm/s and 1800 W, respectively, to build fully dense Cu-W parts. After EB-PBF, cuboid-shaped Cu-W specimens with a dimension of 10 × 10 × 13 mm^3 ($\boldsymbol{x} \times \boldsymbol{y} \times \boldsymbol{z}$, see the coordinate system in Fig. 1) were produced. The lower half parts of the Cu-W cuboids were printed using a constant layer thickness of 100 μm, while the layer thickness was set to 30 μm to build the upper half parts of the samples, keeping the same beam speed and energy. Since the raking procedure during EB-PBF plays a critical role in the particle size distribution and the composition of the raked powder layer, the process parameters used for powder raking were kept constant; i.e., the powder raking was repeated twice, the lifting height of the powder feed tank was twice as much as the layer thickness and the raking speed was kept to 500 mm/s. The reproducibility of the microstructural features derived utilizing different layer thickness values was verified by analyzing different samples printed using the identical process parameters.

To characterize the microstructure, the EB-PBF-built Cu-W samples were cut along the thickness direction, the $\boldsymbol{xz}$-cross-sections (see Fig. 1 for the coordinate system) were polished via ion milling (Leica EM TIC 3X, Germany) and investigated by means of SEM. The distribution of W along the thickness direction was studied using image analysis (ImageJ, National Institutes of Health, USA): an area with a dimension of 9 × 12 mm^2 in the $\boldsymbol{xz}$-cross-section was binarized; this binarized area was then fully covered with horizontal straight lines (parallel to the $\boldsymbol{x}$-direction), each showing width of 1 pixel (dimension in the $\boldsymbol{z}$-direction); the fraction of the tungsten phase on each horizontal line was analyzed pixel by pixel and plotted as a function of the sample height ($\boldsymbol{z}$-direction).

3. Results and discussion

Fig. 2 **a** and **b** depict the particle shape of the pure Cu and the pure W powder used in this work. Owing to its high particle sphericity, the gas atomized Cu powder showed good flowability: The flow rate of the coarse copper powder analyzed utilizing a Hall flow meter with a funnel having an opening diameter of 2.5 mm was measured to be 4.99 g/s. In contrast, the W powder with agglomerates and an irregular particle shape exhibited a poor unmeasurable flowability: During the flowability analysis, the W powder did not flow, even when using a funnel with a large opening with a diameter of up to 10 mm. The LDG measurements depicted in Fig. 2 **c** and **d** reveal a significant difference in the particle size of both elemental powders dispersed in water via stirring: The size of Cu particles is much larger than W particles.

According to the He pycnometry results, the small amount of the powdered sample taken from the powder blend (5 wt % W and 95 wt % Cu) homogenized after 10 min tumbling mixing exhibited a true skeletal density of ~9.22 g/cm^3, which was in good accordance with the theoretical density value; i.e., the powder blend showed a high homogeneity after tumbling mixing. Based on the flowability measurements using a funnel with an opening diameter of 2.5 mm, the Cu-W powder mixture showed a flow rate of 4.87 g/s being comparable to that of the pure copper powder. In Fig. 2 **e**, it is noticed that many huge tungsten agglomerates with a size even larger than the copper particles are observed in the powder blend after mechanical mixing; i.e., the mixing procedure was unable to disintegrate W agglomerates. It is considered that the poor flowability of the W powder and the presence of the numerous W agglomerates in the powder blend could significantly affect the raking procedure and the chemical composition of the raked layer, which will be discussed in the following paragraphs.

Owing to the high energy input, the EB-PBF-processed Cu-W showed a fully dense $\boldsymbol{xz}$-cross-section free of cracks after ion polishing (Fig. 3 **a**). Neither pores nor lack of fusion was detected. The microstructural features are reproducible when using the same parameters during the scan and raking process. According to the microstructure analysis, a clear composition variation in W content along the thickness direction is observed in the EB-PBF-fabricated Cu-W sample printed using various layer thicknesses. In the lower half part built utilizing a layer thickness of 100 μm, a higher amount of the bright phase composed of pure W (according to energy-dispersive x-ray spectroscopy) is detected (Fig. 3 **c**), while the upper part printed using a layer thickness of 30 μm shows less W amount (Fig. 3 **b**), which indicates that the chemical composition along the build direction is controllable, when adjusting the layer thickness values in a targeted manner and using a powder blend

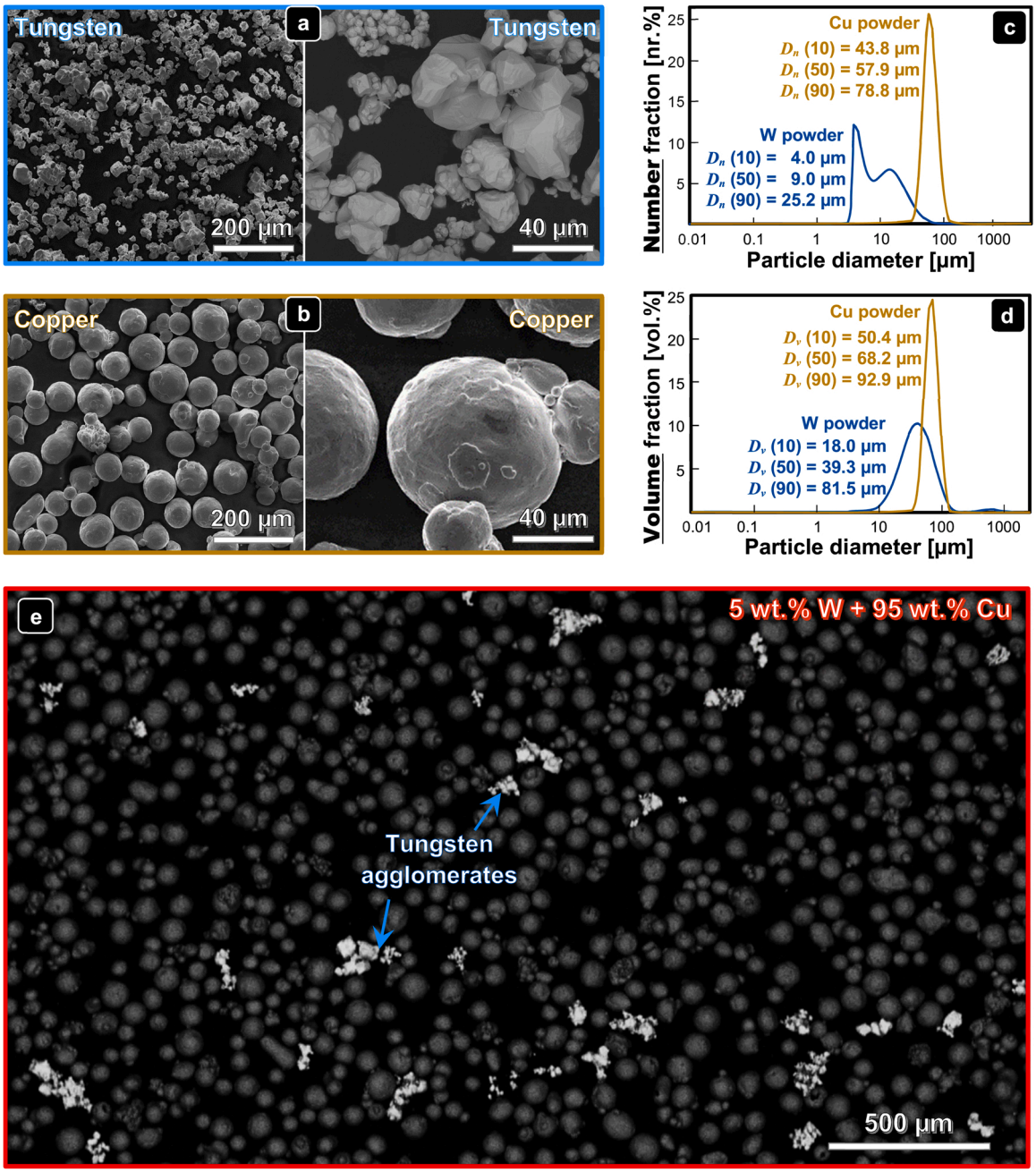

Fig. 2. : Analysis results of the elemental powders and the powder blend, (a) and (b): Representative SEM micrographs showing the particle morphology of the pure Cu and W powders, (c) and (d): Number- and volume-weighted particle size distribution of the Cu and W powders measured by means of Laser Diffraction Granulometry (LDG), (e): Representative SEM micrograph of the homogenized Cu-W powder blend showing numerous W agglomerates.

composed of different powders with significantly different particle size distributions.

Based on the image analysis method explained in Section 2, Fig. 4 shows the W distribution along the build direction in the Cu-W sample built using the selective raking approach. In the upper half part, a relative constant W amount of ~2 % is detected; while the lower half part shows a W fraction of ~6 %. The W content in the lower part is slightly higher than the theoretical nominal W amount in the initial powder blend, which might be caused by the contrast setting of the SEM image and by using the default threshold value for the binarization during image analysis. In addition, during powder raking, a highly dynamic powder hill forms in front of the rake. It is considered that layer thickness is not the single factor that affects the composition of printed parts. Other raking parameters (raking speed, raking repetition and powder feed amount) also play a critical role in the particle size distribution and the composition of the raked powder layer. When setting the lifting height of the powder feed tank twice as much as the layer thickness (as used in this work), finer and heavier particles in the powder hill in front of the rake might tend to sediment, leading to a higher amount of finer particles in the final raked powder layer than expected. In this work, the process parameters used for powder raking were kept constant. The reproducibility of the microstructural features derived utilizing different layer thickness values was verified by analyzing different samples printed using the identical process parameters.

In Fig. 4, it is noticed that a clear transition in the W fraction is observed at the relative height position of 50 %, where the layer thickness was suddenly changed during EB-PBF. The “transition zone”

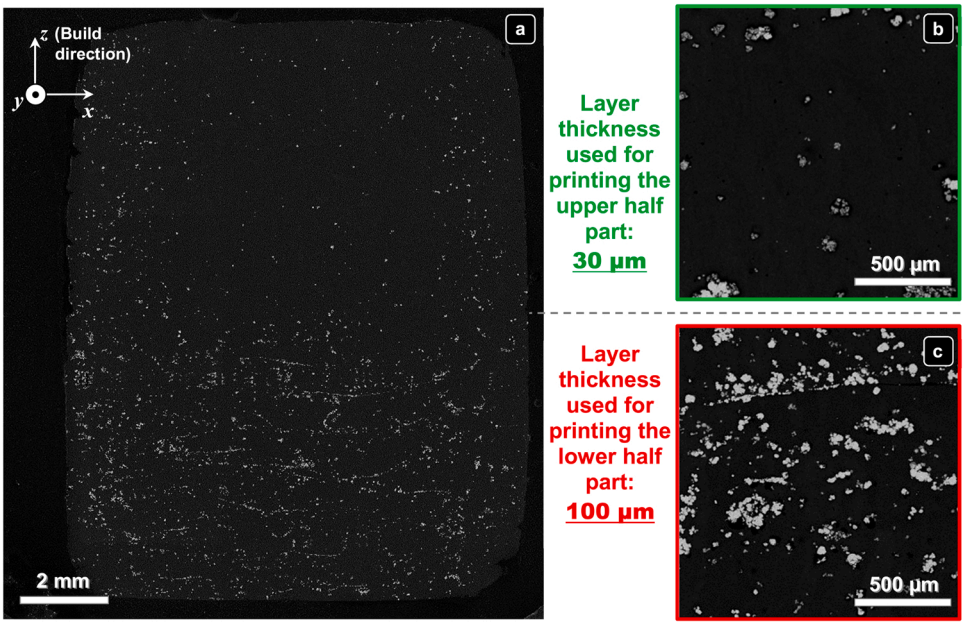

Fig. 3. : SEM micrographs of EB-PBF-produced Cu-W parts. According to energy-dispersive x-ray spectroscopy, the bright phase represents pure W, while the dark phase is almost fully composed of pure Cu, (a): Representative SEM micrograph of the EB-PBF-processed Cu-W with a dimension of $10 \times 10 \times 13$ mm^3 (x × y × z) printed using the selective raking approach. (b): High-magnitude microstructure of the upper part of the Cu-W components printed using a layer thickness of 30 µm. (c): Microstructure of the lower part printed using a layer thickness of 100 µm.

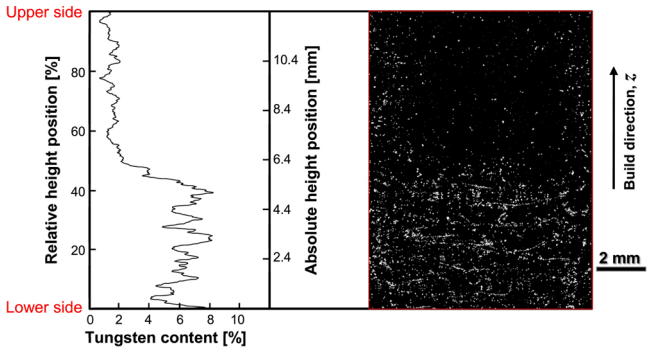

Fig. 4. W content distribution in the EB-PBF-built Cu-W component ($10 \times 10 \times 13$ mm^3) printed using different layer thicknesses. For image analysis, an area with a size of 9×12 mm^2 in the xz-cross-section was selected and binarized, as indicated with the red frame (the white color represents pure W).

shows a width of ~0.5 mm. In order to achieve better controllability of the element distribution, a powder blend composed of powders with narrower particle size distributions (e.g., without agglomerates) that are completely dissimilar from each other (e.g., with less or no overlap) will be used in future work.

In Fig. 4, a relatively narrow variation range in the W fraction (between ~2 % and ~6 %) is observed. However, when comparing this variation range to the W content of 5 wt % in the original powder blend, it is considered that the selective raking procedure presented in this work shows high potential to produce compositionally graded materials exhibiting a larger variation range in the composition of the second phase, if a powder blend containing a higher amount of the second phase is used, which will be investigated in future work. When looking at the microstructure shown in Fig. 4, it is worth noting that the bright phase in the lower part shows some lamellar W ligaments, which are not observed in the upper area. In addition, in the upper half part, a tungsten enrichment is detected near the lateral wall area; while the lower half part exhibits a more homogeneous distribution of W. It is considered that the inhomogeneous W distribution observed in the upper half part might be caused by the surface unevenness of the molten layer due to high energy input when using the layer thickness of 30 µm. Bulging is detected at the top surface in Fig. 3 **a**. Owing to the surface unevenness, more W agglomerates could fill the deepening areas (e.g., lateral edge areas as shown in Fig. 3 **a**) during powder raking, leading to a tungsten enrichment near the lateral wall area.

Furthermore, according to our original idea, more W should be observed in the upper part printed using a low layer thickness of 30 µm: Owing to the much smaller size of W particles (measured by means of LDG, Fig. 2 **c** and **d**), the majority of Cu particles with a bigger size should be removed and more W should remain in the raked layer. Nevertheless, less W was detected in the upper part of the real EB-PBF-produced Cu-W, which seems to be contrary to our original assumption. However, when taking a closer look at Fig. 2 **e**, the low amount of W in the upper part (Fig. 4) can be explained by the presence of numerous W agglomerates in the powder blend, which are much larger than the copper particles as well as the layer thickness of 30 µm, and cannot be disintegrated through mechanical mixing and raking. Moreover, it should be noted that the particle size determined by means of LDG (Fig. 2 **c** and **d**) could be significantly smaller than that of the powder blend after tumbling mixing (Fig. 2 **e**), since the agglomerates could be destroyed via dispersing and stirring the powder in water during LDG analysis. In order to achieve better controllability of the element distribution, a powder blend composed of powders with narrower particle size distributions (e.g., without agglomerates) that are completely dissimilar from each other (e.g., with less or no overlap) will be used in future work.

After EB-PBF, the non-melted powder mixture was sieved, homogenized and analyzed using a helium pycnometer to determine its exact composition. According to the He pycnometry results, the composition of the recycled powder blend could be adjusted by adding additional Cu or W powder. The selective raking approach introduced in this study is not limited to EB-PBF of Cu-W, and can be extended to other powder bed-based AM technologies (e.g., L-PBF and binder jetting) and other material systems (e.g., metal and ceramic composites), in which the constituent elements show limited miscibility or low enthalpy of mixing. The goal of this feasibility study is to “cast a brick to attract jade”, which might open new research perspectives to produce compositionally graded materials using powder bed-based additive manufacturing. In future work, the exact control of the particle size and morphology as well as the number of agglomerates of the fine W powder could lead to a better manipulation of the selective powder raking process. In addition, in order to immediately recycle the powder blend, the definition of a

clear particle size boundary between the fine and coarse constituent powders could help to easily separate the non-melted powders after AM via sieving using appropriate mesh sizes.

4. Conclusion

In this work, Cu-W composite materials, as a simple model material system, with a clear composition variation in W amount along the thickness direction were successfully built by means of **E**lectron **B**eam **P**owder **B**ed **F**usion (EB-PBF) using a powder blend and by varying the layer thickness during the build process. In the initial powder blend, the copper and tungsten powders showed different levels of particle size. When setting a low layer thickness during EB-PBF, the majority of the coarse powder in the powder blend was removed after the raking procedure, which resulted in a higher amount of the fine powder remaining in the raked powder layer. Based on this selective powder raking principle, the chemical composition in each layer was controlled during EB-PBF. According to image analysis, the EB-PBF-built Cu-W composites showed a dense microstructure, a good local microstructural homogeneity and a sharp transition in the chemical composition at the height position, where the layer thickness was varied. In order to improve the controllability of the selective raking approach, the future research focus lies on using a powder blend composed of powders with narrower particle size distributions that are completely dissimilar from each. In addition, other material systems (e.g., metal matrix composites) containing a higher amount of the second phase will be tested to achieve a larger variation range in the composition of the second phase.

CRediT authorship contribution statement

Zongwen Fu: Writing – original draft, Project administration, Methodology, Formal analysis, Conceptualization. **Jihui Ye:** Writing – original draft, Methodology, Investigation, Formal analysis, Conceptualization. **Martin Franke:** Writing – review & editing, Resources, Investigation. **Carolin Körner:** Writing – review & editing, Supervision, Project administration, Funding acquisition, Conceptualization.

Declaration of Competing Interest

The authors declare that they have no known competing financial interests or personal relationships that could have appeared to influence the work reported in this paper.

References

[1] W.E. Frazier, Metal additive manufacturing: a review, J. Mater. Eng. Perform. 23 (6) (2014) 1917–1928.

[2] T.D. Ngo, A. Kashani, G. Imbalzano, K.T. Nguyen, D. Hui, Additive manufacturing (3D printing): a review of materials, methods, applications and challenges, Compos. Part B: Eng. 143 (2018) 172–196.

[3] A. Ramakrishnan, G.P. Dinda, Functionally graded metal matrix composite of Haynes 282 and SiC fabricated by laser metal deposition, Mater. Des. 179 (2019), 107877.

[4] L. Weiss, Y. Nessler, M. Novelli, P. Laheurte, T. Grosdidier, On the use of functionally graded materials to differentiate the effects of surface severe plastic deformation, roughness and chemical composition on cell proliferation, Metals 9 (12) (2019) 1344.

[5] M. Ostolaza, J.I. Arrizubieta, A. Lamikiz, M. Cortina, Functionally graded AISI 316L and AISI H13 manufactured by L-DED for die and mould applications, Appl. Sci. 11 (2) (2021) 771.

[6] C. Körner, Additive manufacturing of metallic components by selective electron beam melting - a review, Int. Mater. Rev. 61 (5) (2016) 361–377.

[7] J. Bieske, M. Franke, M. Schloffer, C. Körner, Microstructure and properties of TiAl processed via an electron beam powder bed fusion capsule technology, Intermetallics 126 (2020), 106929.

[8] D. Wimler, K. Käsznar, M. Musi, C. Breuning, M. Markl, J. Keckes, H. Clemens, C. Körner, S. Mayer, How electron beam melting tailors the Al-sensitive microstructure and mechanical response of a novel process-adapted γ-TiAl based alloy, Mater. Des. 212 (2021), 110187.

[9] J. Zhou, H. Li, Y. Yu, Y. Li, Y. Qian, K. Firouzian, F. Lin, Research on aluminum component change and phase transformation of TiAl-based alloy in electron beam selective melting process under multiple scan, Intermetallics 113 (2019), 106575.

[10] B. Neirinck, X. Li, M. Hick, Powder deposition systems used in powder bed-based multimetal additive manufacturing, Acc. Mater. Res. 2 (6) (2021) 387–393.

[11] C. Andriani, C.K. Chua, Z.H. Liu, D.Q. Zhang, S.L. Sing, C. Andriani, C. Chua, Z. Liu, D. Zhang, S. Sing, Review on melting of multiple metal materials in additive manufacturing, Conference on Progress in Additive Manufacturing (Pro-AM 2014), 2014, p. 175.

[12] C. Anstaett, C. Seidel, Multi-Material Processing: Next step in laser-based powder bed fusion, Laser Tech. J. 13 (4) (2016) 28–31.

[13] C. Guo, W. Ge, F. Lin, Dual-material electron beam selective melting: hardware development and validation studies, Engineering 1 (1) (2015) 124–130.

[14] D. Goll, D. Schuller, G. Martinek, T. Kunert, J. Schurr, C. Sinz, T. Schubert, T. Bernthaler, H. Riegel, G. Schneider, Additive manufacturing of soft magnetic materials and components, Addit. Manuf. 27 (2019) 428–439.

[15] A. Filippov, E. Khoroshko, N. Shamarin, N. Savchenko, E. Moskvichev, V. Utyaganova, E. Kolubaev, A.Y. Smolin, S.Y. Tarasov, Characterization of gradient CuAl–B4C composites additively manufactured using a combination of wire-feed and powder-bed electron beam deposition methods, J. Alloy. Compd. 859 (2021), 157824.

[16] A. Koptyug, M. Bäckström, C. Botero, V. Popov, E. Chudinova, Developing new materials for electron beam melting: experiences and challenges, Mater. Sci. Forum, Trans. Tech. Publ. (2018) 2190–2195.

[17] A. Koptioug, L.-E. Rännar, C.A. Botero Vega, M. Bäckström, V. Popov, Unique material compositions obtained by Electron beam melting of blended powders, Euro PM2018 Congress & Exhibition, Bilbao, Spain, 14–18 October, 2018, European Powder Metallurgy Association, EPMA, 2018.

[18] A. Koptyug, C. Botero, W. Sjöström, E. Jimenez-Pique, A. Şelte, K. Asvik, L.-E. Rännar, M. Bäckström, Steel-based functionally gradient materials obtained via Electron Beam Melting, Alloys for Additive Manufacturing Symposium, AAMS2019, Göteborg, 18–20 September, 2019, 2019.

[19] W. Ge, F. Lin, C. Guo, Functional gradient material of Ti-6Al-4V and γ-TiAl fabricated by electron beam selective melting, Solid freeform fabrication symposium, Tsinghua University, 2015, p. 613.

[20] Y. Qi, X. He, Z.C. Ding, Progresses on development of manufacturing methods of high purity tungsten targets, Mater. Sci. Forum 993 (2020) 414–420.

[21] K.K. Alaneme, B.U. Odoni, Mechanical properties, wear and corrosion behavior of copper matrix composites reinforced with steel machining chips, Eng. Sci. Technol., Int. J. 19 (3) (2016) 1593–1599.

[22] T. Raghu, R. Sundaresan, P. Ramakrishnan, T.R. Rama Mohan, Synthesis of nanocrystalline copper–tungsten alloys by mechanical alloying, Mater. Sci. Eng.: A 304–306 (2001) 438–441.

[23] H. Hashimoto, Z.M. Sun, Y. Inoue, S. Tada, Synthesis of Ti3SiC2 from powder blend of Ti, Si and TiC, J. Alloy. Compd. 426 (1–2) (2006) 263–267.

[24] C. Wang, X.P. Tan, Z. Du, S. Chandra, Z. Sun, C.W.J. Lim, S.B. Tor, C.S. Lim, C. H. Wong, Additive manufacturing of NiTi shape memory alloys using pre-mixed powders, J. Mater. Process. Technol. 271 (2019) 152–161.

[25] A. Kumar, K. Jayasankar, M. Debata, A. Mandal, Mechanical alloying and properties of immiscible Cu-20 wt% Mo alloy, J. Alloy. Compd. 647 (2015) 1040–1047.